Research Article | Vol. 28, No. 23 / 9 November 2020 / Optics Express 34180

Optics EXPRESS

Phase-only modulation with two vertical aligned liquid crystal devices

AUGUSTO ARIAS,[1,2] ALBA M. PANIAGUA-DIAZ,[1,2] PEDRO M. PRIETO,[1] JAVIER ROCA,[2] AND PABLO ARTAL[1,*]

[1] *Laboratorio de Óptica, Centro de Investigación en Óptica y Nanofísica (CiOyN), Universidad de Murcia, Campus de Espinardo (Ed. 34), 30010 Murcia, Spain*
[2] *Voptica S.L., Parque Científico de Murcia, Ctra. de Madrid 388, Complejo de Espinardo – Edificio T, 30100 Murcia, Spain*
[*] *pablo@um.es*

Abstract: Spatial Light Modulators (SLMs) are widely used in several fields of optics such as adaptive optics. SLMs based on Liquid Crystal (LC) devices allow a dynamic and easy representation of two-dimensional phase maps. A drawback of these devices is their elevated cost, preventing a massive use of the technology. We present a more affordable approach based on the serial arrangement of vertical aligned LC devices, with characteristics of phase modulation similar to a widely used parallel aligned LC device. We discuss the peculiarities of the approach, the performance and some potential areas of applications.

1. Introduction

Several advances of the contemporary optics have been boosted thanks to the developments of spatial light modulators (SLMs). These are devices that modify the polarization, amplitude and/or phase of an impinging wavefront. The spatial phase modulation is of particular interest because of the higher transmittance with respect to the amplitude modulation. It has been widely useful in diverse applications such as adaptive optics [1,2], holography [3] or optical micromanipulation [4], among others.

SLMs are commonly composed of a Liquid Crystal (LC) device between two linear polarizers. The type of modulation is given by the orientations of those polarizers. These devices consist of an array of pixels where each pixel is a cell filled with LC molecules with individual control of the electric field through a voltage applied between two electrodes. In Liquid Crystal on Silicon (LCoS) devices, one of the electrodes is transparent and the other serves as a mirror, being operated as reflective displays. Alignment layers are attached to the cell structure in order to control the director axis of molecules along the propagation axis. Thus, liquid crystal molecules in nematic phase, can be vertically aligned (VA), parallel aligned (PA) or twisted (T). SLMs based on T-LCoS devices have been widely used for amplitude modulation due to the polarization rotation originated in a different orientation of the alignment layers. Although those devices can be used for phase modulation as well [5], their implementation requires a complete polarimetric characterization of the LC display and the incorporation of quarter-wave plates. Instead, we will focus on VA- and PA-LCoS devices where alignment layers are parallel to each other.

The dielectric anisotropy or birefringent coefficient, a physical quantity that describes the response of the LC molecules to the applied electric field, is positive in PA-LCoS devices and negative in VA-LCoS devices [6]. In PA-LCoS devices, the molecules are gradually aligned with the applied electric field as its magnitude increases, changing the refractive index exclusively at the orientation of the initial director axis. Those devices are mostly used as phase-only modulators (i.e., with minimal amplitude modulation). In VA-LCoS devices the molecules are initially perpendicular to the alignment layer and they are rotated once the electric field is activated, which are mainly used as high-contrast amplitude modulators [7]. Their phase-only modulation relies

#410429 https://doi.org/10.1364/OE.410429
Journal © 2020 Received 22 Sep 2020; revised 19 Oct 2020; accepted 19 Oct 2020; published 27 Oct 2020

Optics EXPRESS

on the coincidence of the orientation of both polarizer and analyzer with the director axis of the molecules (when the electric field is activated). However, the magnitudes of negative dielectric anisotropy are typically lower than in the case of the positive ones. In consequence, the depth of phase modulation is less than 2π rad, decreasing the diffraction efficiency of the displayed phase maps. Despite those limitations, the use of VA-LCoS devices could be advantageous because their production cost is considerably lower – approximately ten times cheaper – than PA-LCoS devices.

We propose a phase-modulation approach based on VA-LCoS technology with an extended depth of phase modulation. The properties of phase modulation and imaging of two VA-LCoS devices is characterized and compared with the phase modulation of a PA-LCoS with depths of phase modulation higher than 2π rad in the visible spectrum. The applicability of this modulation device for applications in holography and adaptive optics visual simulators is discussed.

2. Methods

2.1. Experimental setup

Figure 1(a) shows the setup to characterize and test the phase modulation of a modulation unit (colored block in the scheme) mainly composed of two VA-LCoS devices (LCoS2 and LCoS3, SYL2282; Syndiant Inc., USA) working in series, comparing it with a PA-LCoS device (LCoS1, PLUTO; Holoeye Photonics AG, Germany). The latter was previously calibrated as described elsewhere [8].

The LCoS devices are illuminated by an expanded and collimated beam from a green diode laser (CPS532; Thorlabs Inc., USA) and the light from a back-illuminated liquid-crystal device (LCD, SYE2271-AS-IMM-00, Syndiant Inc., USA) collimated by the lens L2. The diameter of the illumination is controlled by a diaphragm (AP) acting as iris, being conjugated with LCoS1 by lenses L3 and L4. A horizontal linear polarizer (P1) allows the phase only modulation for the LCoS1. The pupils of LCoS1 and LCoS2 devices are conjugated by the telescope with unitary magnification formed by the lenses L5 and L6. The LCoS2 and LCoS3 are conjugated with a unit-magnification telescope composed by lenses L6 and L7, the 50:50 beam splitters BS1 and BS2 and a spatial filter (F) to reduce diffractive artifacts. The input and output polarization for each VA-LCoS device was set by the linear polarizers P2 and P3 oriented to 45 deg (clockwise from vertical) to achieve phase-only modulation. An achromatic half-wave plate (HWP) was incorporated to increase the light intensity through P3. Thermoelectric modules (TM1 and TM2), each consisting of a thermoelectric Peltier cooler attached to a heat sink, were used to regulate the temperature of the VA-LCoS displays with a precision of 1 °C using the feedback from a sensor incorporated into each element by the manufacturer. The control of the module is carried out by an Arduino board. After the light passes by the LCoS3, optical relay allows the image recording of: the conjugated pupils, by using the CMOS camera CMOS3; the Fraunhofer pattern or the Point Spread Function (PSF) of the programmed phase maps, by using CMOS2; and the visual test projected on the LCD, by using CMOS1. The optical paths for the illumination and acquisition of the laser beam and the light from the LCD are manually switched with foldable mirrors (FMs).

It is important to note that the beam splitter arrangement of the modulation unit is inefficient in terms of energy loss (6.25% maximum transmittance), but was decided for this proof-of-concept experiment to simplify calibration and alignment of the components. In an eventual practical application, small-angle incidence would probably be a better choice even though obliquity had to be taken care of. Moreover, it should take into account that all LCoS devices have some intrinsic losses of light on the generated pattern; therefore, the use of multiple modulators (as in the modulation unit) or the multiple pass by a single one will always be more energy inefficient than the use of a single pass by only one device.

Optics EXPRESS

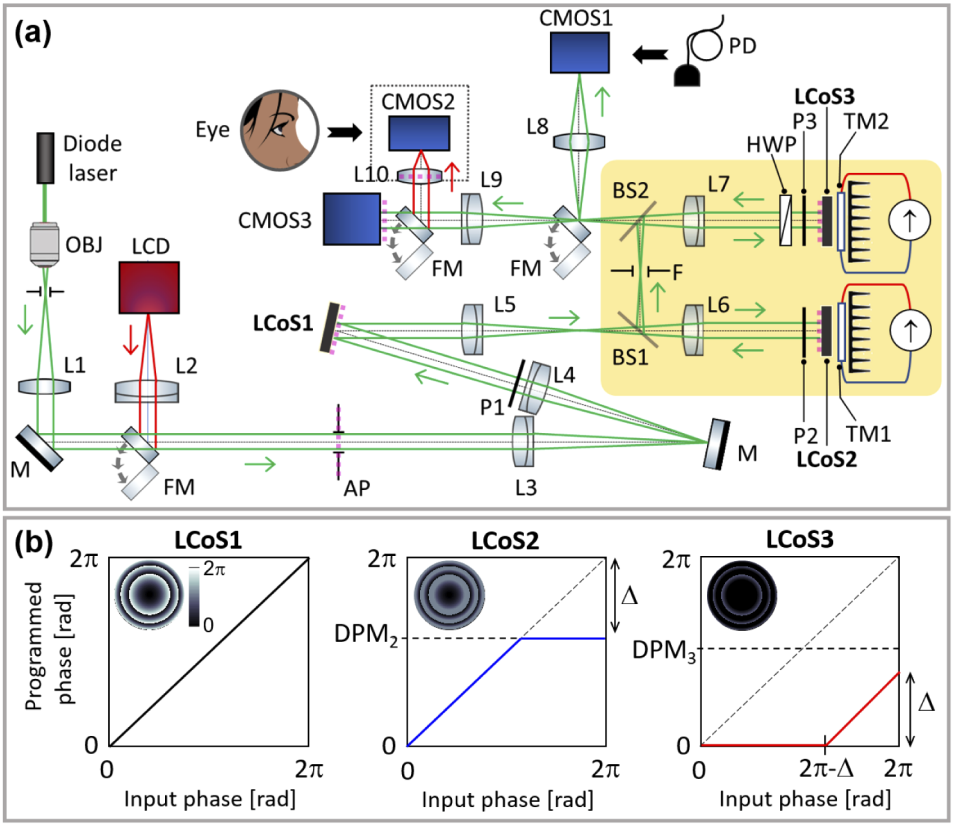

Fig. 1. Setup for the characterization and testing of the phase modulation with VA-LCoS devices. (a) Optical setup for the simultaneous operation of a PA-LCoS device (LCoS1) and two VA-LCoS devices (LCoS2 and 3) in a single modulation unit within the yellow area. The conjugated planes are depicted by the pink dashed lines. OBJ, microscope objective; L1-10, lenses; M, mirror; AP, aperture; FM, foldable mirror; P1-3, linear polarizers; BS1-2, beam splitter; TM1-2, thermoelectric modules; F, field stop; HWP, half-wave plate; CMOS1-3, CMOS cameras; PD, photodiode. (b) Codification of the input wrapped phase for the different LCoS devices. The left graph represents the situation with a standard 2π depth of phase modulator. Central and right graphs show how the total (or input) phase is divided into the two modulators with limited depths of phase modulation (DPM2 and DPM3 for LCOS2 and 3, respectively). Δ is the remaining phase to be modulated by LCoS3.

The codification of phase modulation for each LCoS device is shown in Fig. 1(b). The phase maps to be generated by the PA-LCoS device are wrapped between 0 and 2π rad. Since these devices have a depth of phase modulation of 2π rad, the input phase (or the phase we ask the modulator to display) translates linearly to the programmed phase (the phase that can be loaded in the modulator to display), as shown in the left graph of Fig. 1(b). For the modulation unit based on VA-LCoS devices with limited depth of phase modulation, whereas the input phase is the same as in the previous case, the programmed phase cannot translate completely linearly. Therefore, the programmed phase is firstly represented using the whole depth of phase modulation of LCoS2 (defined as 2π-Δ in the central graph of Fig. 1(b)) and the remaining phase (Δ) is modulated by LCoS3 (see right graph of Fig. 1(b)). This is based on the coherent summation of the optical fields at the conjugated planes where their phases are added while keeping the amplitude constant. The transversal alignment of the displayed phase maps on LCoS2 and 3 was finely adjusted by

Optics EXPRESS

programming a phase map of 2 diopters of defocus. The array displayed on the LCoS2 device was digitally shifted and magnified with respect to that displayed on LCoS3 until the intensity at the zero diffraction order was minimized at the Fraunhofer pattern.

The properties of phase modulation of the LCoS devices were tested and compared by three experiments described below.

2.2. Characterization of phase modulation

First, the temporal response of the generated phase by the LCoS1 and a VA-LCoS (LCoS2) was assessed by using a diffraction-based method [9] where a binary grating with a variable depth (in programmed gray levels) was displayed in each LCoS device while the intensity at the first diffraction order was acquired by a photodiode (PD in Fig. 2(a); PDA36A; Thorlabs Inc., Germany) and digitalized by acquisition card (USB6210; National Instruments, USA) instead of the CMOS1 camera (see Fig. 1(a)). The effective bandwidth of the acquisition system was 11 kHz.

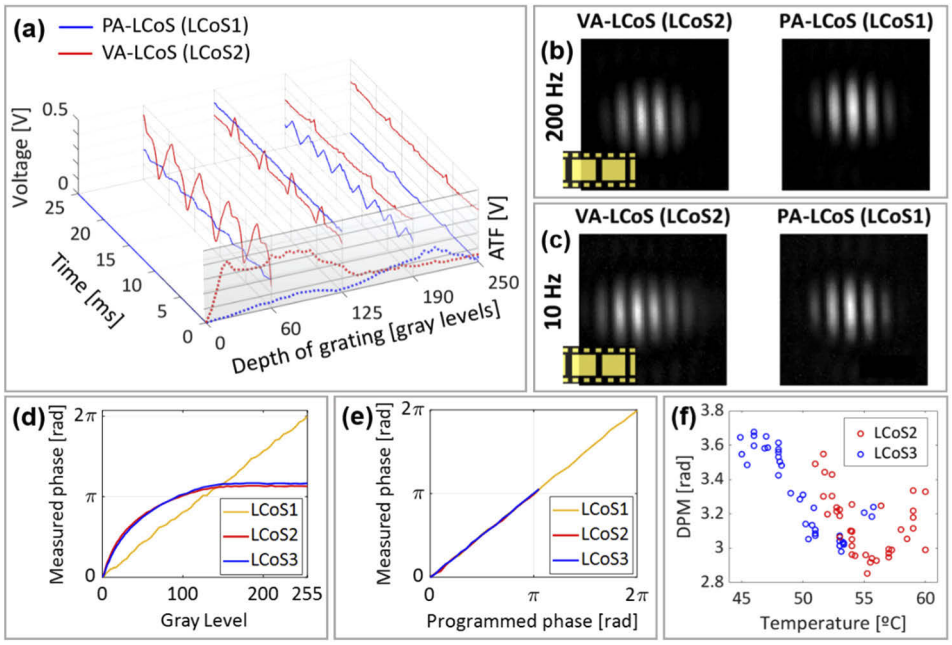

Fig. 2. Characterization of the phase modulation in the LCoS devices. (a) continuous lines, temporal response of the digitalized intensity at the first diffraction order from a binary phase grating; dashed lines on shaded panel, amplitude of the temporal fluctuations (ATF) as function of the grating depth. Young's fringes recorded at: (b) Frame rate of 200 Hz and exposure time of 1 ms, Visualization 1; and (c) Frame rate of 10 Hz and exposure time of 100 ms, Visualization 2. (d) Measured phase as function of the gray levels. (e) Linearized measured phase as function of the programmed one. (f) Dependency of depth of phase modulation (DPM) with temperature in VA-LCoS devices.

The temporal fluctuations of the modulated phase of LCoS1 and LCoS2 were visualized with a Young interferometer [10,11]. An amplitude mask with two holes was placed at the AP plane (see Fig. 1(a)) where each hole was projected on a half of the active area of each display. A gray level of 56 was displayed in one half while the zero gray level was displayed in the other half. The resulting interference at the Fraunhofer plane (i.e., the Young's fringes) were recorded with CMOS1 camera operating at high and low exposure times and frame rates.

Optics EXPRESS

The characterization of the modulated phase as function of the gray levels displayed on each LCoS device was carried out by using the Young interferometer previously described. Thus, for each tested LCoS, the phase induced by the gray levels (from 0 to 2553) programmed on a half of the display was measured respect to the phase induced by a zero gray level programmed on the another half. The resulting Young's fringes were recorded by CMOS1 camera with an exposure time of 50 ms. The shifting of the interferograms was estimated by applying the fast Fourier transform and assessing the phase at the corresponding spatial frequency of the fringes. Although several characterization methods have been developed [12,13], this method was mainly selected by its simplicity. After the characterization, a look-up-table between input gray levels and generated phase value was calculated such that each device accurately adds the programmed phase.

Finally, the depth of phase modulation of LCoS2 and LCoS3 was measured as a function of the temperature in the displays. Temperature was changed via the thermoelectric modules (TM1 and TM2 in Fig. 1(a)).

2.3. Generation of diffractive elements

A diverging lens of 2 diopters and a computer-generated hologram were coded on LCoS1 and the modulation unit, in order to compare their temporal performance and energy efficiency. Camera CMOS1 was set with different exposure times and frame rates. Temporal fluctuations at the position of the reconstructed hologram were assessed by the relative standard deviation, defined as the ratio between the standard deviation and the average intensity during the acquisition time. For all experiments, the size of the exit pupil was 4 mm.

2.4. Generation and compensation of aberrations

The capacity of the proposed modulation approach to generate and correct aberrations was tested and compared with the capacity of the gold standard LCoS1. For the aberration generation experiment, the aberrations were separately programmed on the modulation unit and the standard LCoS1. However, for the aberrations compensation experiment, all LCoS devices were simultaneously operating. While LCoS1 induced the aberrations, the correcting phase map was programmed on the modulation unit.

An object test was displayed in the LCD display, whilst the corresponding blurred and unblurred images were recorded by CMOS2 camera with a frame rate of 8 Hz and exposure time of 125 ms. The corresponding PSFs were also recorded. Three sets of aberrations were programmed. Amplitudes of set 1 and 2 are 1 µm for coma and spherical aberration, respectively. Amplitudes of set 3 are: defocus, −0.6 µm (equivalent to -1 D); coma, 0.5 µm; and spherical aberration, 1 µm. This combination of aberrations and their amplitude are similar to what can be found in a human eye. The generated images were visually inspected by conjugating the eye's pupil with the plane of lens L1 by a channel not shown in Fig. 1(a). To quantitatively assess the quality of those images, the correlation coefficient (CC) between the image without induced aberrations (R) and the blurred or deblurred images (M) was calculated as [14]:

$$\mathrm{CC} = \frac{\sum_{i=1}^{N}(R_i - \bar{R})(M_i - \bar{M})}{\sqrt{\sum_{i=1}^{N}(R_i - \bar{R})^2}\sqrt{\sum_{i=1}^{N}(M_i - \bar{M})^2}} \tag{1}$$

where N is the number of elements of the digitalized images.

Furthermore, the Weber contrast (WC) was also evaluated in each generated image. It is given by:

$$\mathrm{WC} = \left|\frac{I - I_b}{I_b}\right| \tag{2}$$

with I the mean intensity of the optotypes and I_b the intensity of the background.

Optics EXPRESS

3. Results

3.1. Characterized phase modulation

Figure 2(a) shows different temporal fluctuations – or flickering – in the intensity of the first-diffraction order from a binary grating generated with LCoS1 and LCoS2. The main frequencies of these fluctuations are 300 and 180 Hz in LCoS1 and 2, respectively. LCoS2 yields larger amplitude fluctuations than the LCoS1, although this difference is smaller for grating depths higher than 140 in gray levels. According to the dynamic of the intensity signal across the depth of the gratings, while the depth of phase modulation of LCoS1 would be around 2π rad, it is lower in LCoS2. The fluctuations were also observed in Young's fringes (see Figs. 2(b) and 2(c)) when the camera is operating at a high frame rate and short exposure times, 200 Hz and 1 ms respectively, as shown in Visualization 1. However, at a lower frame rate and longer exposure times, 10 Hz and 100 ms respectively, the fluctuations in both devices vanished (see Visualization 2). Flickering in LCoS1 models has been previously investigated and reported [15].

Figure 2(d) depicts the measured phase as a function of gray levels for all LCoS devices. This function follows a nearly linear trend in the case of LCoS1, with a depth of phase modulation of 6.28 rad. On the contrary, for LCoS 2 and 3 the depth of phase modulation and gray levels do not follow a linear function, reaching in this case a maximum depth of phase modulation of 3.55 and 3.66 rad, respectively. After the calibration, the relationships between the programmed (i.e. the phase value sent to the modulator) and measured phase (the phase measured externally) was linear in all devices, as shown in Fig. 2(e). Figure 2(f) exhibits the dependence of the depth of phase modulation with temperature in LCOS2 and 3 whose sensitivities are 0.13 and 0.10 rad/°C, respectively. For further experiments, the temperature of LCoS2 and 3 was fixed to 52 and 47 °C, respectively, using the thermoelectric modules (TM1 and 2 in Fig. 1(a)).

3.2. Generation of diffractive elements

Figures 3(a) and 3(b) show the defocused PSFs captured with different exposure times and frame rates. Temporal fluctuations in the diffraction pattern from both LCoS1 and the modulation unit (LCoS2 and LCoS3) are evident when the camera is operating at high frame rates and short exposure times (see Visualization 3). However, they are minimized as the frame rate is reduced and the exposure time is extended (see Visualization 4). It can be noted that the zero diffraction order of the PSF is brighter in the case of the modulation unit. As a consequence, the diffraction efficiency at the first order is higher for the LCoS1 than the modulation unit (LCoS 2 and 3). The ratio between the defocused energy at the blurred disk and the central peak – measured on unsaturated images –, a quantity related to the diffraction efficiency, is higher in LCoS1 (0.22) than for the VA-LCoS-based modulation unit (0.14).

Figures 3(c) and 3(d) show the reconstructed hologram. The first-diffraction order (i.e., the word 'OPTICS') is brighter when using the standard LCoS1 than when it is generated by the modulation unit. The relative standard deviation of the intensity during the acquisition time at the position marked with the red cross was higher in the modulation unit (0.110) than the LCoS1 device (0.011) when the camera is operating at 26.9 Hz (see Visualization 5). The temporal fluctuations were minimized by synchronizing the LCoS devices and the camera with a frame rate of 60 Hz (see Visualization 6). In that case, the relative standard deviation in the modulation unit and LCoS1 were 0.007 and 0.011, respectively.

3.3. Generation of diffractive elements

Figures 3(a) and 3(b) show the defocused PSFs captured with different exposure times and frame rates. Temporal fluctuations in the diffraction pattern from both LCoS1 and the modulation unit (LCoS2 and LCoS3) are evident when the camera is operating at high frame rates and short exposure times (see Visualization 3). However, they are minimized as the frame rate is reduced

Optics EXPRESS

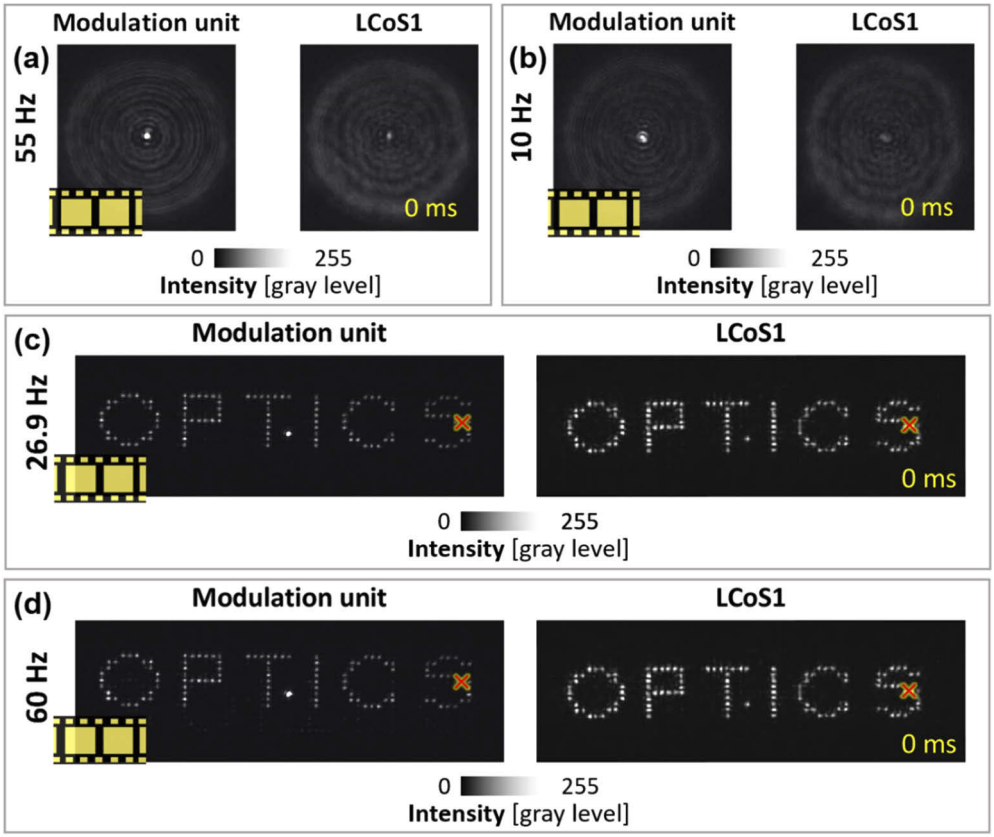

Fig. 3. Diffraction patterns generated by the standard LCoS1 and the VA-LCoS-based modulation unit. Blurred PSF acquired with: (a) an exposure time and frame rate of 1 ms and 55 Hz, Visualization 3; and (b) an exposure time and frame rate of 100 ms and 10 Hz, Visualization 4. Reconstructed hologram acquired with an exposure time of 1 ms and a frame rate of: (c) 26.9 Hz, Visualization 5; and (d) 60 Hz, Visualization 6. Red crosses in (c) and (d) mark the position for the assessment of the temporal fluctuations.

and the exposure time is extended (see Visualization 4). It can be noted that the zero diffraction order of the PSF is brighter in the case of the modulation unit. As a consequence, the diffraction efficiency at the first order is higher for the LCoS1 than the modulation unit (LCoS 2 and 3). The ratio between the defocused energy at the blurred disk and the central peak – measured on unsaturated images –, a quantity related to the diffraction efficiency, is higher in LCoS1 (0.22) than for the VA-LCoS-based modulation unit (0.14).

Figures 3(c) and 3(d) show the reconstructed hologram. The first-diffraction order (i.e., the word 'OPTICS') is brighter when using the standard LCoS1 than when it is generated by the modulation unit. The relative standard deviation of the intensity during the acquisition time at the position marked with the red cross was higher in the modulation unit (0.110) than the LCoS1 device (0.011) when the camera is operating at 26.9 Hz (see Visualization 5). The temporal fluctuations were minimized by synchronizing the LCoS devices and the camera with a frame rate of 60 Hz (see Visualization 6). In that case, the relative standard deviation in the modulation unit and LCoS1 were 0.007 and 0.011, respectively.

Optics EXPRESS

3.4. Generation and compensation of aberrations

Figure 4(a) shows the PSF and image of the visual test without induced aberrations in either modulator. The two-dimensional programmed phase maps are depicted in the first row of Fig. 4(b). The second and third columns show the resulting blurred visual test and PSFs by the VA-LCoS-based modulation unit and the standard LCoS1, respectively. The fourth column shows the deblurred images after the loop of generation/compensation between LCoS1 and the modulation unit, where the compensation was done by simply programming the opposite aberrations on the modulation unit. For each set of aberrations, the morphology of the blurred PSFs as well as the correlation coefficients of the blurred images are similar. Moreover, the deblurred PSFs are similar to the PSF of the system without induced aberrations (Fig. 4(a)) and the correlation coefficient of the corrected images are clearly near to 1. The Weber contrast

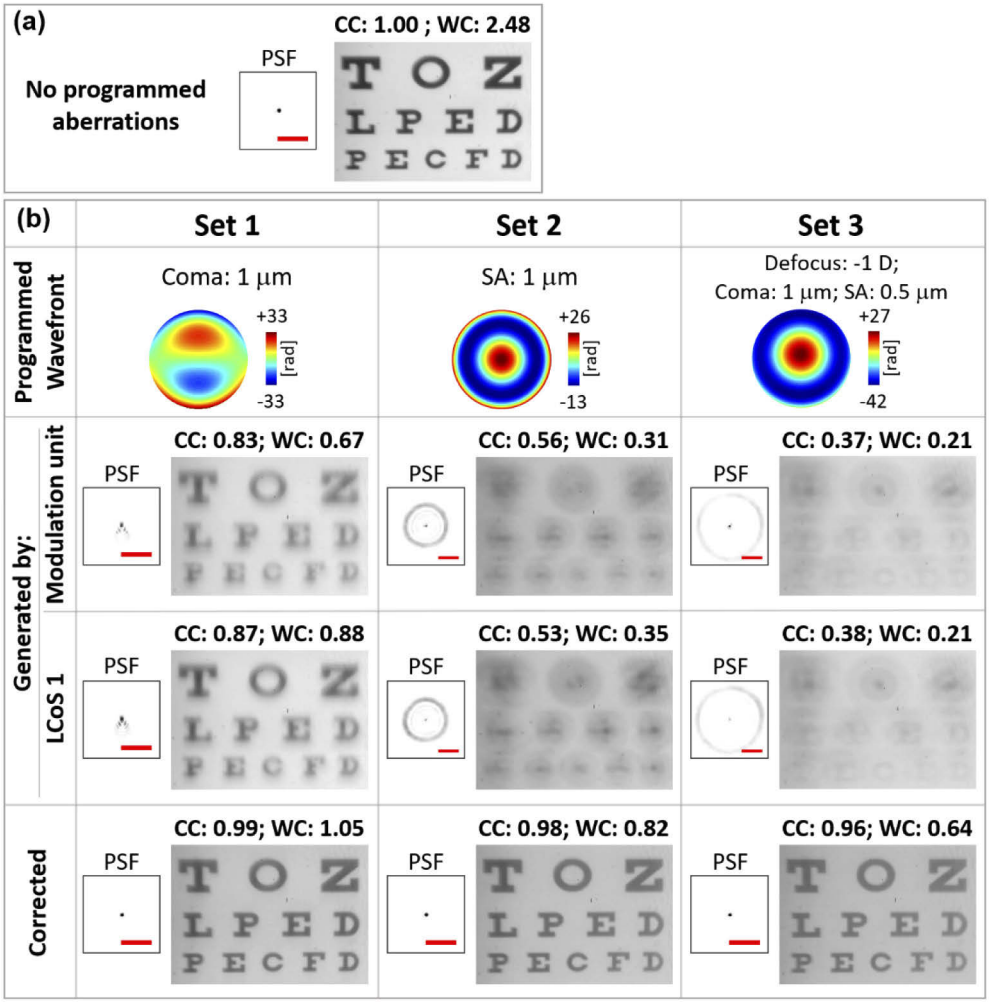

Fig. 4. Generated and corrected aberrated images by the standard LCoS1 and the VA-LCoS-based modulation unit. (a) Image and PSF without programmed aberrations. (b) Blurred and unblurred images and PSFs for each set of aberrations. PSF are the negative version of acquired ones. Dimensions of extended images are 755×1065 µm. Length of red bars is 70 µm. SA, spherical aberration; WC, Weber contrast; CC, correlation coefficient.

Optics EXPRESS

of the blurred images of set 2 are similar to those of set 3. In the case of set 1, the Weber contrast is 24% better in the standard LCoS1 than for the modulation unit. The corrected images present an overall reduction of the Weber contrast up to 42% with respect to the reference image (Fig. 4(a)), despite looking sharp. This reduction of the Weber contrast is a consequence of the lower diffraction efficiency in the modulation unit. After visual inspection, no flickering was observed in the blurred or unblurred images by either LCoS1 device or the modulation unit.

4. Discussion and conclusion

A phase modulation unit based on the use of two VA-LCoS devices optically conjugated have been developed. The properties of phase modulation of this unit were tested and compared with the performance of a standard PA-LCoS device as reference. According to the experimental results (see Fig. 2(a)), the modulation of VA-LCoS presents temporal fluctuations – or flickering – with considerably higher amplitude and lower frequency than standard PA-LCoS. These differences originate in: i. LC viscosity; ii. the digital sequence of voltage in each pixel that each manufacturer uses to represent different gray values; and iii. the frame rate of the LCoS driver. The depth of phase modulation of VA-LCoS devices was slightly higher than π rad with a dependence of the display's temperature, being advisable the use of thermoelectric modules to obtain a steady and reliable depth of phase modulation. The amplitude of the temporal fluctuation is reduced for large gray values in LCoS2, as shown Fig. 2(d). This benefits the performance of the modulation unit due to the adopted scheme of phase codification (see Fig. 1(b)). In other words, the modulation of LCoS3 is less affected by the temporal fluctuations in LCoS2.

The capacity of the VA-LCoS-based modulation unit to reproduce the diffraction patterns with a similar appearance to the generated by the standard LCoS1 was demonstrated through the comparison of the holograms and PSFs shown in Figs. 3 and 4. However, a higher amount of light was deviated to the zero-diffraction order in the modulation unit in comparison to LCoS1 as a consequence of the addressing sequence of voltage and remnant misalignments between the VA-LCoS pupils. Consequently, the modulation unit based on VA-LCoS devices may be not advantageous for holographic applications. Despite this fact, the modulation unit can be a cost-effective solution to be incorporated into visual applications [16–18]. Due to their lower production cost, VA-LCoS modulators have much lower public prices than PA-LCoS. In particular the devices used for this experiment together with the rest of components needed for the modulation unit is within the three-digits cost (not counting bulk buying), ten times cheaper than the PA-LCoS devices.

The contrast of the corrected images between LCoS1 and the modulation unit was reduced (see Fig. 4(b)), although these images are still sharp. On the other hand, the amplitude and the order of the aberrations to be accurately represented and corrected by the modulation unit is limited by the spatial resolution of the telescope between the VA-LCoS displays. Further tests are being conducted to evaluate such limits and the effect of the chromatic aberration induced by the unit.

In conclusion, we demonstrated how two VA-LCoS devices with limited depth of phase modulation can be conjugated and simultaneously operated as a phase modulation unit, generating diffraction patterns very similar to the ones obtained with a PA-LCOS device, with the advantage of a considerably lower price. The main drawback of this modulation unit is that it holds a lower diffraction efficiency at the first-diffraction order and higher amplitude of temporal fluctuation than a PA-LCOS, which might reduce the fields of applications. However, there are fields such as visual adaptive optics where the impact of these drawbacks may be less significant.

Funding

Fundación Séneca (19897/GERM/15); Agencia Estatal de Investigación (PID2019-105684RB-I00); H2020 Innovation In SMEs (H2020-SMEINST2-2016-2017).

Optics EXPRESS

Disclosures

The authors are inventors in a patent application related to this work.

References

1. S. Marcos, J. S. Werner, S. A. Burns, W. H. Merigan, P. Artal, D. A. Atchison, K. M. Hampson, R. Legras, L. Lundstrom, G. Yoon, J. Carroll, S. S. Choi, N. Doble, A. M. Dubis, A. Dubra, A. Elsner, R. Jonnal, D. T. Miller, M. Paques, H. E. Smithson, L. K. Young, Y. Zhang, M. Campbell, J. Hunter, A. Metha, G. Palczewska, J. Schallek, and L. C. Sincich, "Vision science and adaptive optics, the state of the field," Vision Res. **132**, 3–33 (2017).
2. C. Schwarz, P. M. Prieto, E. J. Fernández, and P. Artal, "Binocular adaptive optics vision analyzer with full control over the complex pupil functions," Opt. Lett. **36**(24), 4779–4781 (2011).
3. J. Christmas and N. Collings, "Displays Based on Dynamic Phase-Only Holography," Appl. Sci. **8**(5), 685 (2018).
4. A. Arias, S. Etcheverry, P. Solano, J. P. Staforelli, M. J. Gallardo, H. Rubinsztein-Dunlop, and C. Saavedra, "Simultaneous rotation, orientation and displacement control of birefringent microparticles in holographic optical tweezers," Opt. Express **21**(1), 102–111 (2013).
5. J. L. Martínez, I. Moreno, J. A. Davis, T. J. Hernandez, and K. P. McAuley, "Extended phase modulation depth in twisted nematic liquid crystal displays," Appl. Opt. **49**(30), 5929–5937 (2010).
6. Z. Zhang, Z. You, and D. Chu, "Fundamentals of phase-only liquid crystal on silicon (LCOS) devices," Light: Sci. Appl. **3**(10), e213 (2014).
7. D. Cuypers, H. de Smet, and A. van Calster, "VAN LCOS microdisplays: A decade of technological evolution," J. Disp. Technol. **7**(3), 127–134 (2011).
8. J. L. M. Fuentes, E. J. Fernández, P. M. Prieto, and P. Artal, "Interferometric method for phase calibration in liquid crystal spatial light modulators using a self-generated diffraction-grating," Opt. Express **24**(13), 14159–14171 (2016).
9. Z. Zhang, "Simple method for measuring phase modulation in liquid crystal televisions," Opt. Eng. **33**(9), 3018–3022 (1994).
10. R. Dou, "Simple technique for measuring the phase property of a twisted nematic liquid crystal television," Opt. Eng. **35**(3), 808–812 (1996).
11. A. Bergeron, J. Gauvin, F. Gagnon, D. Gingras, H. H. Arsenault, and M. Doucet, "Phase calibration and applications of a liquid-crystal spatial light modulator," Appl. Opt. **34**(23), 5133–5139 (1995).
12. R. Li and L. Cao, "Progress in Phase Calibration for Liquid Crystal Spatial Light Modulators," Appl. Sci. **9**(10), 2012 (2019).
13. L. Martínez-León, Z. Jaroszewicz, A. Kołodziejczyk, V. Durn, E. Tajahuerce, and J. Lancis, "Phase calibration of spatial light modulators by means of Fresnel images," J. Opt. A: Pure Appl. Opt. **11**(12), 125405 (2009).
14. J. Lee Rodgers and W. Alan Nice Wander, "Thirteen ways to look at the correlation coefficient," Am. Stat. **42**(1), 59–66 (1988).
15. P. A. Cheremkhin, N. N. Evtikhiev, V. V. Krasnov, V. G. Rodin, and S. N. Starikov, "Reduction of phase temporal fluctuations caused by digital voltage addressing in LC SLM "HoloEye PLUTO VIS" for holographic applications," in *Practical Holography XXVIII: Materials and Applications*, H. I. Bjelkhagen and V. M. Bove, eds. (SPIE, 2014), 9006, p. 900615.
16. S. Manzanera, P. M. Prieto, D. B. Ayala, J. M. Lindacher, and P. Artal, "Liquid crystal Adaptive Optics Visual Simulator: Application to testing and design of ophthalmic optical elements," Opt. Express **15**(24), 16177–16188 (2007).
17. L. Hervella, E. A. Villegas, P. M. Prieto, and P. Artal, "Assessment of subjective refraction with a clinical adaptive optics visual simulator," J. Cataract Refractive Surg. **45**(1), 87–93 (2019).
18. C. Cánovas, P. M. Prieto, S. Manzanera, A. Mira, and P. Artal, "Hybrid adaptive-optics visual simulator," Opt. Lett. **35**(2), 196–198 (2010).